

NON-ISOTHERMAL CREEP BEHAVIOR OF A SECOND GENERATION NI-BASED SINGLE CRYSTAL SUPERALLOY: EXPERIMENTAL CHARACTERIZATION AND MODELING

Jonathan CORMIER¹, Xavier MILHET¹, François VOGEL², José MENDEZ¹

¹Laboratoire de Mécanique et de Physique des Matériaux ; Ecole Nationale Supérieure de Mécanique et d'Aérotechnique
1 Avenue Clément Ader ; 86960 Futuroscope Chasseneuil ; France

²Turboméca – SAFRAN group; 64511 Bordes; France

Keywords: Very high temperature creep, Burner rig, Dislocations, γ' dissolution/precipitation, Creep modeling

Abstract

In order to simulate emergency regimes possibly encountered by turboshaft engines for helicopter, non-isothermal creep behavior of the second generation single crystal Ni-Based superalloy MC2 was investigated. These tests were performed with one short overheating at 1200°C during the isothermal creep life of the material at 1050°C. Overheatings were carried out using a burner rig designed to achieve temperature jumps as fast as 60°C/s in the range 1050°C-1200°C. Both the overheating duration and its position during the isothermal creep life at 1050°C of the material have a great effect on the non-isothermal creep behavior. The modifications in creep behavior were clearly linked with microstructural evolutions occurring during temperature changes, e.g: the dissolution of the γ' phase on heating the material and the dislocation recovery processes.

Based on these microstructure characterizations, a classical macroscopic model involving isotropic variables and a von Mises criterion was enhanced with the addition of new internal variables representative of the γ' -volume fraction and a recovery function attesting for the dislocation activity.

Introduction

Single crystal nickel-based superalloys are widely used for the hottest part of jet engines such as high pressure turbine blades, where creep resistance is one of the operating life limiting factors. During a flight, turbine blades should not deform a lot as blade failure, or more likely blades touching the external housing generally leads to their damage in the engine. It is generally accepted that the entire turbine blade should not be permanently strained over 1% during operating life [1]. This critical deformation takes into account a wide range of thermal/mechanical loadings ranging from very high temperature/low stress in blade tips to low temperature/high stress in blade roots. Actually, Ni-based single crystal superalloys exhibit superior creep resistance at temperature as high as 1100°C [2] due to their particular microstructure, consisting of 70% in volume of coherently precipitated γ' cubes ($L1_2$ lattice) separated by thin channels of face centered cubic (fcc) γ matrix [3]. Extensive literature is devoted to the study of their properties, especially on isothermal creep over a wide range of stress and temperature [4-11]. Two temperature/stress domains can be distinguished: (1) at low temperature ($T < 950^\circ\text{C}$) and high stress, no significant evolution of the initial optimal microstructure occurs during the creep experiment, while (2) at higher temperature/lower stress, great modifications of the microstructure are observed during primary creep stage: rafting of the γ' phase perpendicular to the applied stress for negative γ/γ'

misfit alloys and development of stable dislocation networks at the γ/γ' interfaces.

However, these studies cannot describe entirely the mechanical behavior of the material during a real flight since both stress and temperature are likely to vary depending on the engine rating. For example, emergency conditions such as a One Engine Inoperative (OEI) event can be encountered and are very different from the regular cruising regime. When an OEI event occurs on a twin-engine helicopter, the remaining engine must provide enough power to maintain the helicopter airborne. In this case, the high pressure turbine blades of the remaining engine experience a sharp temperature jump from 1050°C to 1200°C during the time needed to recover almost regular cruising conditions. This produces non-isothermal creep conditions with the load only slightly increasing as the engine speed increases slightly, while the temperature varies due to the OEI simulation. In this context, long exposures of superalloys to extreme temperature are well documented in the literature [5, 13-17]: it provokes the dissolution of the γ' reinforcing phase and induces a severe loss in mechanical properties. In contrast, little is known about the mechanical behavior when the material is exposed to very high temperature transients, particularly when under load. For an engine designer, modeling the mechanical behavior of the superalloy during non-isothermal creep is essential to guarantee the engine integrity and to adopt best maintenance procedures. Yet, these materials were not designed originally to sustain such severe conditions. In particular, creep behavior and creep life after the OEI is of great interest. However, being able to reproduce realistic operating conditions in well-controlled laboratory conditions for various thermal and mechanical histories is a challenging issue, whether in terms of experimental characteristics (heating rate control and temperature levels), material characterization and mechanical modeling. The purpose of this paper is to address these issues by detailing: (1) a test bench specifically developed to simulate an OEI, (2) the non-isothermal creep behavior in relation to microstructure evolutions and finally, (3) a mechanical model based on a classical macroscopic approach, modified to attest for the microstructure evolutions. This study is particularly devoted to the second generation Ni-base superalloy MC2, currently in operation in various engines.

Experimental techniques

Creep tests and simulation of the OEI

The simulation of realistic flight conditions in a laboratory is a challenging issue, especially when complex thermal/load conditions are involved in components such as blades. However, it is a critical issue to understand fundamental aspects of the

mechanical behavior of superalloys in their real environment. In fact, the experimental set-up has to reproduce as accurately as possible the harshest conditions encountered by turbine blades, i.e. very high temperature (up to 1200°C), oxidizing environment and creep tensile stress around 140 MPa. Moreover, to meet the OEI specifications, the experimental set-up needs to be able to jump within seconds from 1050°C, corresponding to regular cruising conditions, to 1200°C, corresponding to emergency rating. Therefore, an OEI can be simply simulated by a specific non-isothermal creep test procedure: a jump in temperature from 1050°C to 1200°C has to be performed in the course of an isothermal creep test at 1050°C/140 MPa. In this context, both pre-OEI and post-OEI creep conditions are pure isothermal creep at 1050°C/140MPa and the OEI simulation (1200°C/140MPa + $\Delta\sigma$) happens after a certain amount of pre-creep. However, if the test seems fairly practical, it turns out to be a challenging issue due to the temperature levels and heating/cooling rates. Generally, creep tests are performed using either radiant or resistance furnaces. Unfortunately, in the OEI context, these two types of furnaces have very limited performances when dealing with temperature as high as 1200°C, especially due to their slow temperature jump ability between 1050°C and 1200°C. While it is not problem at 1050°C where the volume fraction of γ' phase is close to 60% at thermodynamic equilibrium, a slow temperature jump toward higher temperature leads to massive γ' dissolution [12], leading to a substantial modification of the behavior of the material. The heating rate of resistance furnaces in the temperature range considered in this study is only few degrees per minute, which makes it totally useless for studying the effect of an OEI on the material behavior. Radiant furnaces seem to be a little more capable to be used for the simulation of an OEI since they can achieve heating rates as high as 10°C/s. However, cooling rates over 1°C/s are difficult to obtain with this type of furnace at the temperature levels considered in this study. During the time needed to cool down the material to 1050°C, massive dissolution of the γ' reinforcing phase takes place first, followed by a delayed reprecipitation of cubic nanometric precipitates in the γ channels [13]. In this context, failure is observed within minutes after the overheating has occurred [14].

Based on these limitations, a specific test rig (STR) was designed to meet the requirements of the OEI simulations. It is a modified version of a test rig used to study the cooling of combustion chamber using multiperforated plates, equipped with a device applying a static tensile stress on the material during the entire non-isothermal creep experiment. Both very high temperature and very fast heating rates are achieved using a hot gas flow obtained by burning highly pressurized kerosene in a combustion chamber. The temperature of the hot gas flow, monitored using a thermocouple, is directly controlled by the pressure of the kerosene inlet. Using this configuration, heating and cooling rates as high as 60°C/s can be expected. The specimen, heated up by forced convection, is loaded in a testing zone located at a sufficient distance from the flames to ensure homogeneous temperature of the gas flow and to prevent any contact with the flames. The temperature of the specimen is monitored using pyrometric measurements. In order to limit the specimen drag due to the gas flow velocity ($\approx 100 \text{ ms}^{-1}$), a specific prismatic geometry was chosen with dimension $1.5 \times 14 \text{ mm}^2$ (Figure 1). Using this geometry, the aerodynamic stress, estimated around 1.5 kPa, can be neglected in front of the tensile creep stress ($\approx 140 \text{ MPa}$).

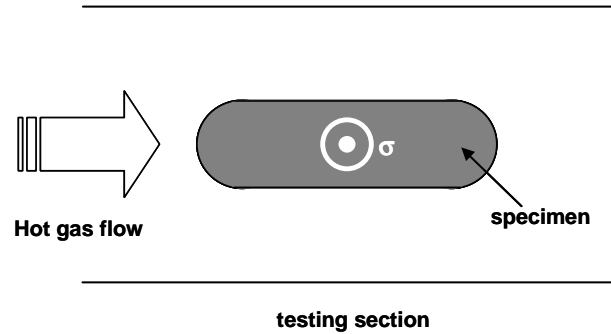


Figure 1. Schematic illustration of the testing section of the STR in top view. The prismatic geometry is chosen to limit the specimen drag in the gas flow. The centered circle indicates the stress axis.

Up to this point, the STR simulates a turboshaft engine in terms of temperature (up to 1230°C), heating and cooling rates (up to 60°C/s), and environment (kerosene burnt gas). It is therefore able to perform well-controlled non-isothermal creep tests with reasonably fast heating rates to be representative of OEI conditions. However, due to technical limitations, the STR can sustain only few hours at 1050°C while a typical creep test in these conditions last at least 500h. The STR is therefore only used to perform the OEI simulation. Both pre-OEI (t_{pre}) and post-OEI (t_{post}) creep at 1050°C are performed using a classical creep rig equipped with a radiant furnace using a special procedure including rigorous thermal control, developed to ensure the reliability of the non-isothermal creep tests. At the end of the pre-OEI creep, the material is cooled down under load to avoid any evolution of the deformation microstructure. The specimen is then loaded in the STR. The testing procedure during the OEI consists of: (1) ignition of the flame to reach 1050°C after few seconds, (2) applying a tensile stress $\sigma_0 + \Delta\sigma$ to the specimen at 1050°C for 1min (3) performing a jump from 1050°C to 1200°C by increasing the pressure of injection of kerosene and maintaining this regime for durations ranging 30s to 150s, (4) cooling the material down at room temperature at 60°C/s under load to preserve the deformation microstructure developed during the OEI. At this step, the specimens gauge lengths are systematically measured to deduce the plastic strain cumulated during the OEI simulation. Finally, the material is reloaded in the classical creep rig for the post-OEI creep until failure. Special care was taken to control the thermal conditions at the beginning of this last stage in order to limit the microstructure evolutions possibly occurring during the temperature stabilization.

Material and specimens

MC2 is a second generation nickel-based superalloy developed by ONERA for gas turbine applications operating at high temperature ($T > 900^\circ\text{C}$). Its weight composition is given in Table 1. As-grown material was solution heat treated at 1305°C for 3 hours and air quenched, to dissolve all the γ' phase particles formed by eutectic reaction during solidification and to reduce chemical segregations. It was then aged for 6 h at 1080°C and air quenched followed by 20 h at 870°C and air quenched to control both the γ' size ($\approx 0.4 \text{ }\mu\text{m}$) and to achieved the best creep resistant microstructure i.e. γ' content around 70% in volume (Figure 2). This microstructure will be called the as-received state of the

material. Creep specimens, 14 mm gauge length with a prismatic section 4 mm wide and 1.5 mm thick, were machined from single crystal rods with orientation within 5° off [001] along the strain axis, secondary orientation being both parallel to the gauge side and perpendicular to the gauge axis (see Figure 1).

Element	Ni	Cr	Co	W	Ta	Al	Mo	Ti
Wt %	Bal	8	8	8	6	5	2	1.5

Table 1. MC2 nominal composition.

Microstructure characterizations

Microstructure evolutions occurring during non-isothermal creep were performed on dedicated specimens, by interrupting the tests either at the end of the pre-OEI creep or just after an OEI or in the course of the post-OEI creep test. A JEOL JSM 7000F scanning electron microscope (SEM) operating in the range 9 – 25 kV was used to observed the microstructure evolution. SEM samples were mechanically polished until a mirror finish was obtained. Selective dissolution of the γ phase by electrochemical polishing of the surface using a triacid solution (vol. %) 45% H_2SO_4 , 42% HNO_3 and 13% H_3PO_4 was then performed to reveal details of the γ/γ' microstructure. Dislocation substructures were analyzed using a Philips CM 20 transmission electron microscope (TEM) operating at 200 kV. TEM samples were cut perpendicularly to the strain axis $\langle 001 \rangle$ corresponding to the dislocations habit plane. Cell sizes of the dislocation networks were estimated by measuring the mean diameter of dislocation cells inscribed circles. The average cell size results from at least 200 measures.

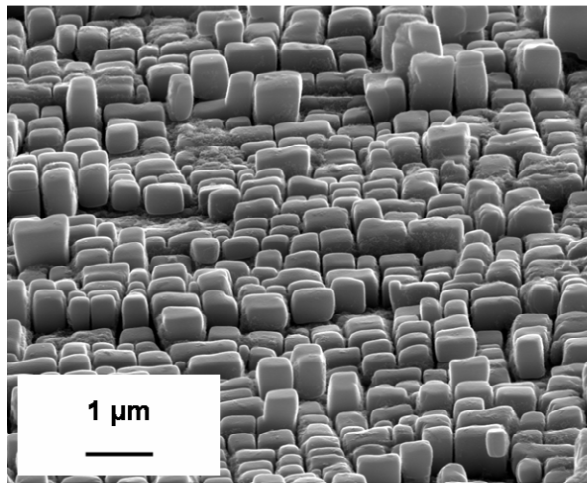


Figure 2. As-treated γ/γ' microstructure of MC2 alloy (tilted at 70°).

Experimental results

Non-isothermal creep behavior

Typical non-isothermal creep behavior corresponding to the OEI simulation is represented in Figure 3. In this example, the first part of the creep curve corresponds to $t_{pre} = 100h$ and is analog to the typical isothermal behavior at 1050°C/140MPa. At the end of t_{pre} , the simulation of the OEI lasted for $t_{OEI} = 150s$. Surprisingly, the post-OEI creep stage t_{post} (1050°C/140MPa), exhibits the

typical primary, steady-state and tertiary stages. As for isothermal conditions, once the tertiary stage is initiated, the material fails rapidly. Therefore, this stage will be neglected in the following, since it is far beyond useful application of the material. As a conclusion, the OEI is not “too harmful” since neither failure nor massive plastic strain were observed during or just after it and the material could sustain post-OEI creep for hours before failure.

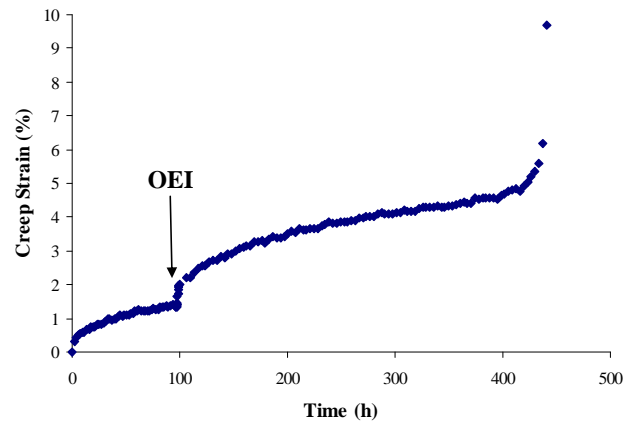


Figure 3. Non-isothermal creep behavior with $t_{pre} = 100h$ and $t_{OEI} = 150s$.

From Figure 3, as a first striking result, the material can sustain a much higher deformation amplitude at the end of the post-OEI steady-state creep stage than that possibly achieved in pure isothermal conditions i.e. 1% approximately [15]. As a second striking result, the material deforms for the same amount of strain (approximately 1%) during the post-OEI steady-state creep life but the primary amplitude increases along with t_{OEI} (see for example Figure 4). These results are true for any t_{OEI} and any t_{pre} . As a consequence, longer t_{OEI} leads to larger overall plastic strain than shorter t_{OEI} , solely due to the very large difference in post-OEI primary creep amplitude. In other words, the OEI softens the material i.e. it can sustain much higher strain amplitude than what could have been reached in pure isothermal conditions because of a larger plastic strain during the post-OEI creep life.

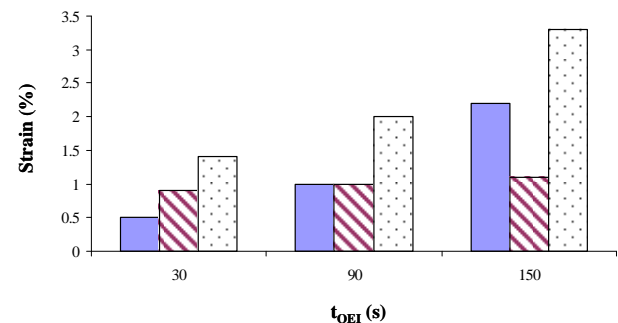


Figure 4. Comparison between strains in the various stages of post-OEI creep for different t_{OEI} . (Grey bar: primary creep stage; Striped bar: steady-state; Dotted bar: total deformation at the tertiary onset). Steady-state strains are identical for any t_{OEI} .

Figure 5 plots the evolution of the logarithm of the strain rate against time for non isothermal creep tests with various t_{OEI} .

According to Figure 5, the strain rate of the post-OEI steady-state is accelerated compared to its pre-OEI (i.e. pure isothermal) counterpart. As a third striking result, longer t_{OEI} leads to slower post-OEI steady-state strain rate. For example, the post-OEI minimum creep rate is $\dot{\epsilon}_{\min-150s} = 1.8 \cdot 10^{-8} s^{-1}$ after $t_{OEI} = 150s$ while it is twice as fast e.g. $\dot{\epsilon}_{\min-30s} = 3.6 \cdot 10^{-8} s^{-1}$ after $t_{OEI} = 30s$. As a consequence, longer t_{OEI} always leads to longer post-OEI residual creep lives t_{post} except for $t_{pre} = 0$. This result derives simply from the fact that the time needed to reach the same amount of post-OEI steady-state strain (e.g. 1%) is shorter with faster strain rate. In the case of $t_{pre} = 0$, as a fourth striking result, t_{OEI} has no effect on both the overall creep life and steady-state creep rate, which are surprisingly identical to those in pure isothermal condition. However, in this condition, the OEI on as-received material still softens it since the overall strain at the end of the steady-state is larger than that measured for isothermal conditions.

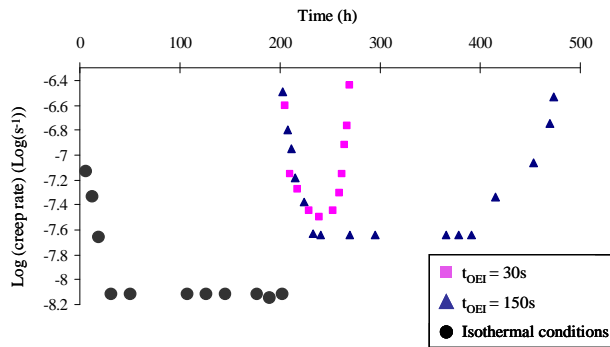


Figure 5. $\log(\dot{\epsilon})$ vs time. Longer t_{OEI} leads to slower minimum strain rate than a shorter one. Both are faster than isothermal minimum creep strain rate

Microstructure evolutions

Microstructure modifications occurring in the course of non-isothermal creep tests were analyzed after interrupting the test at the end of t_{pre} , just after the simulation of the OEI or after some time spent in t_{post} . Figure 6 shows examples of the effect of an OEI (with $t_{OEI} = 90s$ or $150s$) performed after $t_{pre} = 50h$, corresponding to a fully rafted microstructure. Starting from a γ' raft area fraction $f_{\gamma'}$ close to 60% at the end of t_{pre} (Figure 6a), the overheating at $1200^{\circ}C$ produces massive γ' dissolution, especially for longer t_{OEI} (Figure 6b, c). In this case, $f_{\gamma'}$ can be as low as 35% (Figure 6c). Along with the rafts dissolution, the matrix channels grow larger, their width increasing approximately from 200 nm to 500 nm with increasing t_{OEI} . However, in agreement with literature [16-19], the supersaturated γ matrix channels fill up with fine γ' cubic precipitates upon cooling just after the OEI (see [14, 15] for illustrations of this hyperfine reprecipitation in case of non-isothermal creep). After subsequent post-OEI creep, both original $f_{\gamma'}$ and γ channel width are recovered, so that the initial microstructure is rebuilt. No small γ' precipitates remain in the matrix channel (Figure 6d).

Along with the γ' raft evolution, the dislocation networks located at the γ/γ' interface evolve as well. Figure 7 represents the evolution of the dislocation networks during non-isothermal

creep. Figure 7a shows the typical dislocation networks developed during isothermal conditions at $1050^{\circ}C/140MPa$ during secondary creep stage. Figures 7b to 7d show the dislocation networks after various overheating times. By measuring the dislocation cell sizes, it appears that the OEI provokes an increase of cell size for any t_{OEI} compared to the cell size measured after isothermal creep. However, longer t_{OEI} leads to smaller cell size along with a smaller standard deviation. No large evolution of the cell size was noticed during post-OEI creep. It is only slightly reduced but never reaches the pre-OEI value.

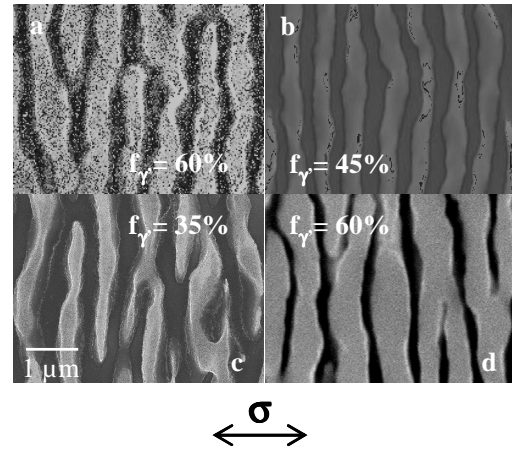


Figure 6 Evolution of the γ' rafts during non isothermal creep (γ' rafts are in light grey) a) raft microstructure after $t_{pre} = 50h$ at $1050^{\circ}C/140MPa$, b) raft microstructure after $t_{pre} = 50h + t_{OEI} = 90s$, c) raft microstructure after $t_{pre} = 50h + t_{OEI} = 150s$, d) raft microstructure after $t_{post} = 142h$

Non isothermal creep modeling

Modeling microstructural evolutions

Viscoplastic behavior of single crystal superalloys are usually modeled using constitutive equations which account for the effects of the applied stress σ_0 and of several damaging mechanisms (such as increase of pore density, oxidation, increase of mobile dislocations, precipitates coarsening ...) [7, 20]. Temperature dependence of the viscoplastic behavior is only described through the evolution of the material's constants used in these laws. These constants have to be identified for each temperature of interest.

A classical approach to describe creep is the Chaboche law [21].

This approach gives the evolution of the creep strain rate $\dot{\epsilon}_p$ using the concept of internal stress σ_i (Eq. 1).

$$\dot{\epsilon}_p = \left(\frac{|\sigma_0 - X| - R - R_0}{K} \right)^n \text{Sgn}(\sigma_0 - X) \quad (1)$$

In this equation, the internal stress ($\sigma_i = X + R + R_0$) is the sum of isotropic and kinematic hardenings, respectively R and X (null at the beginning of the mechanical loading) and of R_0 the initial internal stress considered as isotropic. K and n are mechanical constants depending on both the temperature and the mechanical loading σ_0 .

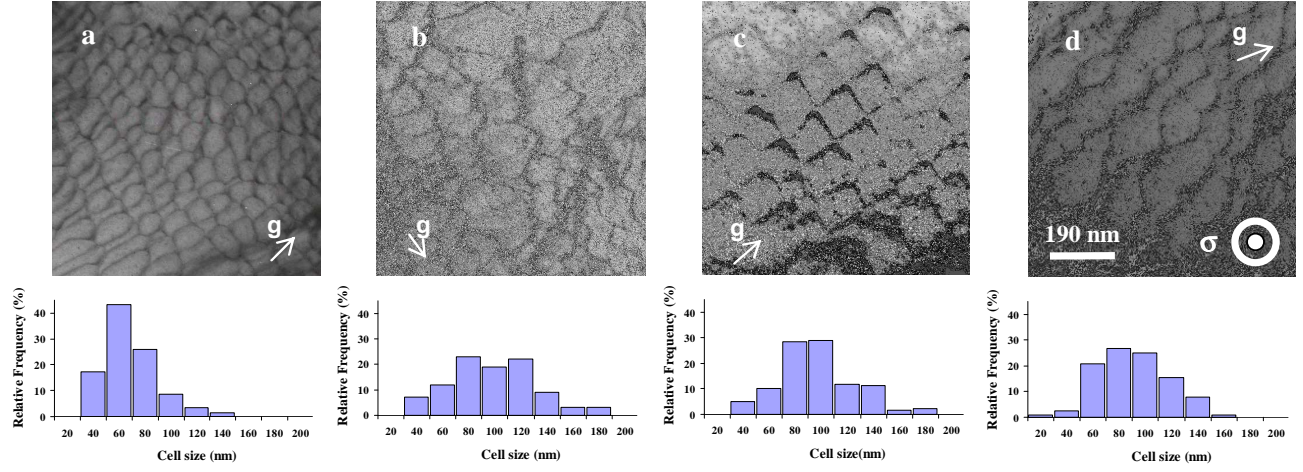


Figure 7. TEM bright field ($g = 002$, $B = [001]$) illustrating the evolution of the dislocation networks cell morphology at the γ/γ' interfaces and their corresponding bar charts representing the cell size distribution for a) isothermal conditions during secondary creep stage b) after $t_{OEI} = 30s$ c) after $t_{OEI} = 90s$ d) after $t_{OEI} = 150s$.

For the description of the uniaxial creep strain along a particular direction of a single crystal (the $[001]$ orientation in our case), a simpler form of equation 1 can be used by removing the kinematic hardening X , keeping only isotropic hardening R . A nonlinear form of R is chosen with an exponentially saturating function (Eq. 2) of the cumulated creep strain in order to describe the relatively long secondary creep regimes (regardless of creep lives) of single crystal Ni-based superalloys at high temperature ($T > 1000^\circ C$) and low stress [4]. This formulation of isotropic hardening accounts for the fact that throughout the primary creep regime, strain hardening gradually increases due to the combined effects of dislocation motion in the matrix corridors (work hardening) and γ' precipitate rafting [22, 23]. Saturation of R attests for creep steady-state. It corresponds to an equilibrium value of the dislocation density in the matrix channels of superalloys [24]. At this point, the creep behavior of the material is mainly dominated by recovery processes such as dislocation climb along γ/γ' interfaces of the rafted structures or γ' cutting by dislocations, which was recently identified as creep rate controlling in Re-containing superalloys [25, 26].

$$\dot{R} = b(Q - R)\dot{\epsilon}_p \quad (2)$$

Starting from this classical formalism for isothermal creep modeling, it was chosen to modify it for non-isothermal creep since an OEI produces transient microstructure evolutions. In these conditions, equations 1 and 2 with parameters identified for $1050^\circ C$ and $1200^\circ C$, the temperatures reached during non-isothermal creep, are useless since these constants will only be representative of the equilibrium creep conditions. It was therefore chosen to introduce new internal variables and hardening (softening) in the isothermal creep behavior to attest for the microstructure evolutions during overheatings which allows the model to capture transients in the mechanical behavior.

The principle of this model, based on pioneering works on high temperature fatigue of IN100 superalloy [27], consists of the quantification of microstructure deviation from the equilibrium

with time. Two main features were identified to control the non-isothermal creep behavior:

- the evolution of $f_{\gamma'}$, the volume fraction of γ' -strengthening phase during and after the OEI simulation
- the evolution of the dislocation structures at γ/γ' interfaces

As shown in the experimental section, dissolution of the γ' phase softens the material. Therefore, it can be assumed that the progressive recovery of its γ' phase equilibrium value f_{eq} hardens it. In this context, the deviation of $f_{\gamma'}$ from its equilibrium f_{eq} in the vicinity of overheatings can be seen as a variation of the yield strength of the material. In order to account for macroscopic softening/hardening effects, the internal variable R^* was introduced in equation 1. Furthermore, kinematic hardening in equation 1 is still neglected since it is assumed that both γ' phase dissolution and precipitation is isotropic. The variation of creep strain rate for non-isothermal creep can be written as follows:

$$\dot{\epsilon}_p = \left(\frac{\sigma_0 - R - R_0 - R^*}{K} \right)^n \quad (3)$$

Since the macroscopic hardening/softening is linked with the deviation of $f_{\gamma'}$ from its equilibrium value f_{eq} , it is assumed that R^* directly depends on $f_{\gamma'}$, the γ' -volume fraction at any time (Eq. 4):

$$R^* = -\frac{R^*}{\tau_r} + \alpha(f_{\gamma'} - f_{eq}) \quad (4)$$

where

$$\dot{f}_{\gamma'} = \frac{f_{eq} - f_{\gamma'}}{\tau} \quad (5)$$

In these equations, f_{eq} is the γ' -volume fraction at equilibrium at the tested temperatures equal to 0.6 and 0.3 at $1050^\circ C$ and $1200^\circ C$, respectively [12]. τ is a thermodynamic time constant

being equal to τ_d , characteristic of the dissolution of the γ' -phase on heating the material at 1200°C under load, and τ_r , characteristic of the recovery of the γ' -microstructure by precipitation and coalescence processes when back at 1050°C. Based on data available in the literature [12, 28], the dissolution time constant τ_d and the γ' -recovery time constant τ_r used in equation 5 were determined: τ_d was actually measured for cubic and rafted γ' -microstructure while τ_r was only measured in case of rafted structure [12, 15, 28].

As observed in the experimental section, the dislocation networks are modified by the OEI and can be seen as recovery. In this context, a recovery function $g = b_v(Q_v - R)$ was introduced in the isotropic hardening R (Eq. 2) to model the effects of the dislocation structure evolutions. This results in equation 7.

$$\dot{R} = b(Q - R)\dot{\epsilon}_p + b_v(Q_v - R) \quad (7)$$

Such a modeling approach is usually chosen to describe the evolution in creep properties of aged superalloys where, for example, precipitates sizes can increase by Ostwald ripening processes [29, 30]. In our case, the function g attests for modification of dislocation networks at the γ/γ' interface after an OEI has occurred.

Modeling identification and results

Isothermal identifications of the behavior of the material at 1050°C and 1200°C (e.g: n , K , Q , b , R_0 parameters of equations 1 and 2) have been carried out using results extracted from tensile tests conducted under different strain rates to enhance the viscoplastic behavior [28]. A step by step optimization comparing numerical simulation with a given set of parameters to experimental results was conducted using the optimizer module of the finite element code Zebulon.

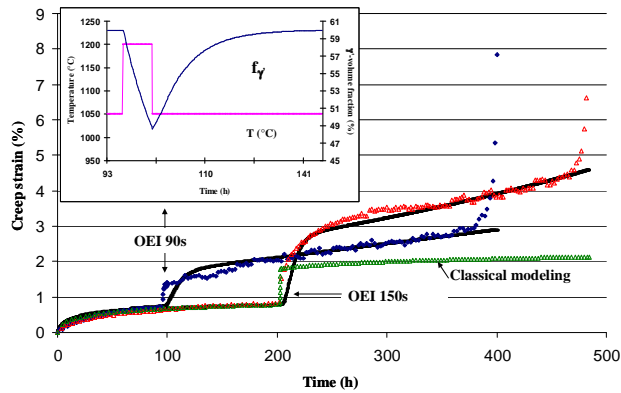


Figure 8. Modeling of the non-isothermal creep behavior (bold lines) for a 90s OEI (respectively a 150s OEI) introduced at $t_{pre} = 98h$ (resp. $t_{pre} = 200h$) and compared to their respective experimental curves (dotted lines). The evolutions of the γ' -volume fraction ($f_{\gamma'}$) and of the temperature (T °C) as a function of a non-linear scaled time in the case of the 90s OEI is given as an insert. For sake of comparison, modeled creep curve with a classical approach is given in the case of the 150s OEI.

In case of non-isothermal conditions, new parameters τ_d , τ_r and f_{eq} were directly determined from microstructure observations [12, 15] while the parameters α , b_v and Q_v have been optimized from a wide range of non-isothermal creep tests, such as the one presented in Figure 3, with different t_{pre} and t_{OEI} .

Figure 8 illustrates two results of the non-isothermal modeling compared with the experimental results. There is excellent agreement between modeled and experimental curves for each case, with post-OEI primary creep regimes and increased stationary creep strain rates well described. Predictions from the classical modeling using equations 1 and 2 with their respective constants at 1200°C during the OEI and at 1050°C during the rest of the non-isothermal creep life, show a great departure from the experimental curve, especially during post-OEI creep where microstructure has evolved. Indeed, as these materials' constants were identified in isothermal conditions, they may not be representative of these evolutions presented in previous sections of this article. Therefore, such a modeling approach provides a real breakthrough for the prediction of material deformation under non-isothermal conditions inducing microstructural changes.

Discussion

During isothermal creep at high temperature/low stress, it is generally accepted that the primary creep stage ends when the rafting process is completed and dislocations networks at the γ/γ' interfaces are well established [5, 22, 23, 31]. However, in the case of non-isothermal conditions, a primary creep stage is systematically observed at the beginning of post-OEI creep whether the microstructure is built with γ' cubes ($t_{pre} = 0$) or with γ' rafts with well-developed dislocations networks at the γ/γ' interfaces. The rafting process can therefore be ruled out for being directly involved during the post-OEI primary creep stage. However, as observed in Figure 6, massive dissolution of the γ' phase occurs during the OEI simulation at 1200°C, promoting the widening of the γ matrix channels. During post-OEI creep, the equilibrium γ' volume fraction f_{eq} at 1050°C (60%) is recovered after few hours. Based on the results given by the model, it is seen that a simple approach, in terms of a temporarily deviation of $f_{\gamma'}$ from f_{eq} due to the OEI, reproduces fairly well the new post-OEI primary creep stage (see insert Fig. 8). According to the model, the post-OEI primary stage lasts for approximately the time needed to recover f_{eq} at 1050°C. At a microscopic level, the OEI simulation reduces temporarily the Orowan stress σ_{or} along with the transient modification of $f_{\gamma'}$, over the time necessary for both γ' rafts and γ channels to recover their initial width during the post-OEI creep at 1050°C. Indeed, to propagate into the γ channels, dislocations need to overcome the Orowan stress [32, 33]:

$$\sigma_{or} = \sqrt{\frac{2}{3}} \frac{\mu \times b}{w} \quad (8)$$

where μ is the shear modulus, b is the Burgers vector and w is the channel width. In this context, a large plastic deformation is expected at the beginning of the post-OEI creep stage since larger γ channels (increase of w) allow easier matrix dislocation motion due to a drop of σ_{or} . This should even be enhanced for longer t_{OEI} . However, the deformation rate will eventually slow down along with the recovery of f_{eq} . In this context, longer primary

stage results from larger deviation from f_{eq} caused by longer t_{OEI} . It seems therefore reasonable to assume that the primary creep stage is closely linked to the deviation from f_{eq} for a given temperature at the microscopic level. The amplitude may also be closely linked to the diffusion kinetics of chemical elements in the material to rebuild the pre-OEI microstructure.

During the isothermal steady-state creep stage at high temperature/low stress, the microstructure is built with stable γ' rafts and well-developed dislocation networks at the γ/γ' interfaces. At a microscopic level, an internal stress σ_i builds up in the γ channels, and can be described as follows:

$$\sigma_i = \sigma_{sol-sol} + \sigma_{bs} + \sigma_{or} \quad (9)$$

where $\sigma_{sol-sol}$ is the solid solution hardening, σ_{bs} is the back stress induced by dislocation networks and σ_{or} is the Orowan stress due to the γ' rafts. It was reported in literature that under isothermal high temperature/low stress conditions, only a limited number of matrix dislocations can enter the γ channel due to σ_{bs} [34], and that further deformation is only possible if dynamic recovery of these matrix dislocations occurs by γ' cutting events [26, 35, 36]. It was suggested by these authors that the minimum creep rates $\dot{\epsilon}_{min}$ directly result from the number of γ' cutting events. As a result, for isothermal conditions, a stress increase leads to faster $\dot{\epsilon}_{min}$. The problem is that in our case, the applied stress remains constant throughout the test and post-OEI $\dot{\epsilon}_{min}$ may vary depending on both t_{OEI} and t_{pre} . However, as proposed in the model, the recovery function g has to be introduced in order to describe the post-OEI steady-state stage. This recovery function attests directly for a larger dislocation activity in the matrix channels according to [34]. As a first assumption, it can be postulated that the OEI simulation results in a virtual increase of the applied stress in post-OEI creep. Actually, this would explain satisfactorily the increase of post-OEI $\dot{\epsilon}_{min}$ when the OEI is performed on a microstructure built with rafts. However, this fails to explain the behavior when the OEI is performed on as-received material, where $\dot{\epsilon}_{min}$ remains the same as in isothermal conditions. Therefore, this first assumption can be ruled out. As a second assumption, the OEI may modify the internal stress σ_i of the material as proposed in the model section, where R_0 , in equation 3, corresponds to $\sigma_{sol-sol}$. Since an OEI performed on as-received material does not modify $\dot{\epsilon}_{min}$ compared to its pure isothermal counterpart, it can be assumed that both terms σ_{or} and $\sigma_{sol-sol}$ in equation 9 are hardly affected by an OEI, at least after that $f\gamma'$ recovers its equilibrium f_{eq} . It is therefore assumed that OEIs may only greatly impact σ_{bs} , the backstress resulting from the dislocations in the matrix channels. As shown in the experimental result section, shorter t_{OEI} leads to larger dislocation cell sizes irregularly distributed i.e. lower dislocation density at the γ/γ' interfaces. This probably derives from the fact that for longer time spent at 1200°C, the microstructure gets closer to its equilibrium at this temperature. In this context, it is assumed that the internal stress is smaller for shorter t_{OEI} , allowing more dislocations to enter the γ matrix channels during subsequent creep at 1050°C. According to previous studies [26, 35, 36], this leads to an increased minimum strain rate. This assumption is also

in full agreement with the experimental results obtained for an OEI performed at $t_{pre} = 0$, where minimum creep rates do not depend on t_{OEI} . In this case, the microstructure exhibits neither γ' rafts nor dislocation networks at the γ/γ' interfaces and σ_i reduces simply to the sum of $\sigma_{sol-sol} + \sigma_{or}$. In this context, σ_i should not be substantially modified by the OEI. This is also well predicted by the model [37], for this condition ($t_{pre} = 0$) which was not used as an input for the identification of the model parameters.

Conclusion

The non-isothermal creep behavior of MC2 single crystal Ni-based superalloy was studied in conditions representative of in-service One Engine Inoperative (OEI) events possibly encountered on turboshaft engines for helicopters. Overheatings at 1200°C under load were introduced in the course of the creep life of the material at 1050°C using a burner rig especially adapted for the purpose of these experiments, enabling temperature jumps as fast as 60°C/s. The main consequences of such temperature jumps under these thermal and mechanical conditions are:

- a decrease of the overall creep life of the material.
- a modification of the creep behavior with a new primary regime right after the OEI and an increase of the post-OEI stationary creep rate compared to that before.

The experimental results show that an OEI simulation modifies the primary creep amplitude compared to its isothermal counterpart, independently of the microstructure of the material. This amplitude increases with increasing the OEI duration t_{OEI} . OEI simulation also modifies the minimum creep rate which is increased compared to isothermal conditions. In addition, these minimum creep rates depend on t_{OEI} in a surprising way: longer t_{OEI} leads to slower minimum creep rates if the OEI is performed on a fully rafted microstructure. If OEIs are performed on as-received material, minimum creep rates equal the ones measured for isothermal conditions. Finally, the plastic deformation at the onset of the tertiary stage depends solely on the primary stage amplitude, steady-state stage deformation amplitude being constant.

This non-isothermal creep behavior was clearly shown to be dependant on both the dissolution/precipitation/coalescence of the γ' -phase during overheatings for the new primary creep regime, and on the modification of the dislocation density at the γ/γ' interfaces for the post-OEI secondary creep regime.

Based on these microstructural evolutions, a viscoplastic Chaboche law was modified by introducing two new internal variables, for the evolutions of the γ' phase volume fraction, and by adding a recovery function, for the evolution of the dislocation density. This model is predictive of the creep strains encountered during non-isothermal creep until the transitions with the tertiary regime, whatever the OEI length and position in the creep life at 1050°C of the material.

Acknowledgements

The authors gratefully acknowledge Turboméca –SAFRAN group and la DGA for financial support. We especially thank Professor G. Caillaud for judicious advices in modeling approaches, Dr J.-L. Champion and Dr P. Villechaise for their help in several experiments.

References

1. F. Lubahn, *Plasticity and Creep of metals* (New York: Wiley, 1968).
2. D. Fournier. "Acquis, Besoins, Espoirs", (Paper presented at Colloque National Superalliages Monocristallins, Toulouse, 1995), 7.
3. M. Benyoucef et al., "In situ deformation experiments on a γ/γ' superalloy - Strengthening mechanisms", *Materials Science and Engineering*, A234-236 (1997), 692-694.
4. P. Caron. "High γ solvus new generation nickel-based superalloys for single crystal turbine blade applications", (Paper presented at Superalloys 2000, Warrendale, PA, 2000), 737-746.
5. R.C. Reed et al., "Creep of CMSX-4 superalloy single crystals: effects of rafting at high temperature", *Acta mater*, 47 (12) (1999), 3367-3381.
6. N. Matan et al., "Creep of CMSX-4 superalloy single crystals: effects of misorientation and temperature", *Acta mater*, 47 (5) (1999), 1549-1563.
7. D.W. MacLachlan and D.M. Knowles, "Creep-behaviour Modelling of the Single-Crystal Superalloy CMSX-4", *Metallurgical and Materials Transactions A*, 31A (May) (2000), 1401-1411.
8. P. Caron et al., "On the effects of heat treatments on the creep behaviour of a single crystal superalloy", *Scripta Metallurgica*, 20 (6) (1986), 875-880.
9. G.L. Drew et al. "Single crystal superalloys: the transition from primary to secondary creep", (Paper presented at Superalloys 2004, Seven Springs, 2004), 127-136.
10. F. Diologent, "Comportement en fluage et en traction de superalliages monocristallins à base de nickel", (Ph.D. thesis, Université de Paris Sud, Centre d'Orsay, 2002).
11. D.W. MacLachlan and D.M. Knowles, "Modelling and prediction of the stress rupture behaviour of single crystal superalloys", *Material Science and Engineering*, A302 (2001), 275-285.
12. J. Cormier, X. Milhet, and J. Mendez, "Effect of very high temperature short exposures on the dissolution of the γ' phase in single crystal MC2 superalloy", *Journal of Materials Science*, 48 (18) (2007), 7780-7786.
13. T. Grosdidier, A. Hazotte, and A. Simon, "Precipitation and dissolution processes in γ/γ' single crystal nickel-based superalloys", *Material Science and Engineering*, A256 (1998), 183-196.
14. J. Cormier, X. Milhet, and J. Mendez, "Anisothermal Creep at very high temperature of a second generation Ni-based single crystal superalloy", *Materials Science and Engineering*, A483-484 (2008), 594-597.
15. J. Cormier, X. Milhet, and J. Mendez, "Non-isothermal creep at very high temperature of the Nickel based single crystal superalloy MC2", *Acta Materialia*, 55 (18) (2007), 6250-6259.
16. G.L. Erickson. "The development and application of CMSX-10", (Paper presented at Superalloys 1996, Warrendale, 1996), 35-44.
17. S. Duval et al., "Phase composition and chemical order in the single crystal base superalloy MC2", *Acta Metall. Mater*, 42 (1) (1994), 185-194.
18. K. Kakehi, "Influence of secondary precipitates and crystallographic orientation on the strength of single crystals of a Ni-based superalloy", *Metallurgical and Materials Transactions A*, 30A (May) (1999), 1249-1259.
19. A.M. Brass, D. Roux, and J. Chene, "Role of secondary γ' precipitation and of hydrogen in the first stage of the plastic deformation of the γ matrix of a Ni base superalloy single crystal", *Material Science and Engineering*, A323 (2002), 97-102.
20. M. Mclean and B.F. Dyson, "Modelling the effects of damage and microstructural evolution on the creep behaviour of engineering alloys", *Journal of engineering Materials and Technology*, 122 (2000), 273-278.
21. J.-L. Chaboche, "Calcul des déformations viscoplastiques d'une structure soumise à des gradients thermiques évolutifs", (Ph.D. thesis, Orsay, 1972).
22. R.C. Reed, D.C. Cox, and C.M.F. Rae, "Damage accumulation during creep deformation of a single crystal superalloy at 1150°C", *Materials Science and Engineering*, A 448 (2007), 88-96.
23. T. Sugui et al., "Aspects of primary creep of a single crystal nickel-base superalloy", *Material Science and Engineering*, A262 (1999), 271-278.
24. M. Probst-Hein, A. Dlouhy, and G. Eggeler, "Interface dislocations in superalloy single crystal", *Acta Mater*, 47 (8) (1999), 2497-2510.
25. G. Malzer et al., "Miniature specimen assessment of creep of the single crystal superalloys LEK 94 in the 1000°C temperature range", *Metallurgical and Materials Transactions A*, 38A (2007), 314-327.
26. A. Kostka et al., "L1₂-phase cutting during high temperature and low stress creep of a Re-containing Ni-base single crystal superalloy", *Journal of Materials Science*, 42 (2007), 3951-3957.
27. G. Cailletaud and J.-L. Chaboche. "Macroscopic description of the microstructural changes induced by varying temperature: example of the IN 100 cyclic behaviour", (Paper presented at Third International Conference on Mechanical Behaviour of Materials (ICM-3), Cambridge (G.B.), 1979).

28. J. Cormier, "Comportement en fluage anisotherme à haute et très haute température du superalliage monocristallin MC2", (Ph.D. thesis, Université de Poitiers, 2006).
29. J. Lemaitre and J.L. Chaboche, *Viscoplasticity - Modelling of particular effects in Mechanics of Solid Materials* (Cambridge: Cambridge University Press, 1990), 328.
30. J.-L. Chaboche and G. Cailletaud. "Loi de comportement en non-linéaire et exemples sur matériaux métalliques", (Paper presented at Journées à thème ADDL - Fondements et implantation des lois de comportement élastoplastiques en éléments finis, Paris-Bercy, 2002).
31. J.X. Zhang et al., "The effect of lattice mismatch on the dislocation motion in superalloys during high-temperature low-stress creep", *Acta mater*, 53 (2005), 4623-4633.
32. T.M. Pollock and A.S. Argon, "Creep resistance of CMSX-3 nickel base superalloy single crystals", *Acta Metall. Mater*, 40 (1) (1992), 1-30.
33. K. Serin et al. "A kinetic study of γ -channel widening during high temperature and low stress creep of superalloy single crystals", (Paper presented at EUROMAT 2000, Tours, France, 2000), 1303-1308.
34. A. Dlouhy, M. Probst-Hein, and G. Eggeler, "Static dislocation interactions in thin channels between cuboidal particles", *Material Science and Engineering*, A309-310 (2001), 278-282.
35. G. Eggeler and A. Dlouhy, "On the transformation of $\langle 010 \rangle$ -dislocations in the γ -phase of superalloy single crystals during high temperature low stress creep", *Acta mater*, 45 (10) (1997), 4251-4262.
36. R. Srinivasan, G.F. Eggeler, and M.J. Mills, " γ' -cutting as a rate-controlling recovery process during high temperature and low-stress creep of superalloy single crystals", *Acta mater*, 48 (2000), 4867-4878.
37. J. Cormier et al., "Non-isothermal creep behavior modeling of Ni-based single crystal superalloys under very high temperature/low stress conditions", To be published.